Comparison of flowability and sinterability among different binder jetting feedstock powders: nanopowder, micropowder, and granulated powder

Wenchao Du [a], Guanxiong Miao [b], Zhijian Pei [a], and Chao Ma [a,b,c,1]

[a] Department of Industrial & Systems Engineering, Texas A&M University, College Station, TX

[b] Department of Mechanical Engineering, Texas A&M University, College Station, TX

[c] Department of Engineering Technology & Industrial Distribution, Texas A&M University, College Station, TX

Abstract

Feedstock powders used in binder jetting additive manufacturing include nanopowder, micropowder, and granulated powder. Two important characteristics of the feedstock powders are flowability and sinterability. This paper aims to compare the flowability and sinterability of different feedstock powders. Three powders were compared: nanopowder (with a particle size of ~100 nm), micropowder (with a particle size of 70 μm), and granulated powder (with a granule size of ~70 μm) made from the nanopowder by spray freeze drying. Flowability metrics employed included apparent density, tap density, volumetric flow rate, mass flow rate, Hausner ratio, Carr index, and repose angle. Sinterability metrics employed included sintered bulk density, volumetric shrinkage, and densification ratio. Results show that the granulated powder has a higher flowability than the nanopowder and a higher sinterability than the micropowder. Moreover, different flowability metric values of the granulated powder are close to those of the micropowder, indicating that these two powers have a comparably high flowability. Similarly, different

[1] Corresponding author: cma@tamu.edu

sinterability metric values of the granulated powder are close to those of the nanopowder, indicating that these two powders have a comparably high sinterability.

1 Introduction

Additive manufacturing (AM), also known as 3D printing, has many advantages, including the elimination of special tooling, flexible and customizable design, and efficient usage of raw materials. Binder jetting is one of the seven AM technologies defined by ASTM and ISO [1]. When binder jetting is used to fabricate a part, a powder bed is first formed, then a green part is created by selectively jetting a liquid binder onto the powder bed, and finally the green part is densitified by sintering [1]. Advantages of binder jetting include complimentary support and ease of debinding [2,3]. The feedstock powders used in binder jetting include nanopowder (or submicron powder) [4–7], micropowder [8–14], and granulated powder [7,15–23]. Granulated powder is often prepared from nanopowder, and the granule size is usually in the micrometer range [21–23].

Flowability, the ability of a powder to freely flow, is crucial for uniform powder spreading and thus homogeneous microstructure in green and sintered parts [2]. A flowability comparison can help select a suitable feedstock powder to avoid spreading-induced defects in the powder bed and consequently in green and sintered parts. Flowability is a result of a complex combination of material properties. Particle size is a critical variable that determines the powder flowability [2]. There are some studies in the literature on comparing the flowability among different feedstock powders. For example, Miao et al. [7] investigated the effect of granulation on the powder flowability. By comparing the raw nanopowder and granulated powder using various flowability metrics, it was concluded that the granulated powder had a higher flowability than the raw

nanopowder. In other studies, flowability was compared across micropowders with different particle sizes [8–14]. Flowability was also compared across granulated powders from different granulation processes [15,16], such as spray drying and milling in Suwanprateeb et al.'s study [15]. Moreover, the effects of granule composition on various flowability metrics of granulated powder were reported [17–21]. However, knowledge gaps exist in the literature for the flowability of binder jetting feedstock powders. First, the flowability of granulated powder has not been compared with that of micropower of a similar size. In addition, the hierarchical (intragranular and intergranular) packing structure of granulated powder has not been considered in the flowability comparison.

Sinterability, the ability of the powder to be densely sintered, is often used to compare the sintering performance of different powders under similar packing conditions [2,3]. A sinterability comparison can help select a suitable feedstock powder to achieve a desired printed and sintered density. Sinterability is usually characterized from pressed samples to ensure similar packing conditions across different powders. For example, a granulated powder was prepared by spray drying from a tricalcium phosphate powder mixed with a polyvinyl butyral powder as a binder [18]. The effect of fraction of binder added to the granulated powder on its sinterability was studied by pressing and sintering. Using the same approach (i.e., pressing and sintering), the effects of granulation parameters and granule size on the sinterability of granulated powder prepared by spray freeze drying were studied [22]. However, sinterability has not been compared across different types of binder jetting feedstock powders, i.e., nanopowder, micropowder, and granulated powder.

This research aims to fill the aforementioned three knowledge gaps about flowability and sinterability of the feedstock powders used in binder jetting. In this study, a granulated powder

with a granule size of ~70 μm was prepared by spray freeze drying from a nanopowder with a particle size of ~100 nm. The granulated powder, the nanopowder, and a third micropowder with a particle size of 70 μm were compared using various flowability and sinterability metrics. The hierarchical packing structure of granulated powder was considered when comparing its apparent density and tap density with those of other two powders. Conclusions were drawn based on the comparison results.

2 Methods

2.1 Materials

Alumina nanopowder (90-187085) was acquired from Allied High Tech, USA. Alumina micropowder (26R-8S70) was acquired from Inframat, USA. The particle morphology of these two powders was characterized by a scanning electron microscope (SEM, TESCAN VEGA II LSU, Czech Republic). The particle size distribution of the micropowder was acquired by analyzing its SEM images with ImageJ. The volume-weighted mean particle size of the micropowder was then obtained.

2.2 Preparation of granulated powder

Spray freeze drying [7,22] was chosen as the granulation method in this study. A slurry with a solid loading of 20 vol.% was prepared from the nanopowder described above. The preparation started with adding water and alumina milling balls into a high-density polyethylene bottle with a capacity of 1000 mL. To decrease the slurry viscosity, an ammonium salt of an acrylic polymer (Dispex AA 4040 NS, BASF, Germany) was added as a dispersant, followed by a manual shaking to evenly mix the dispersant with the water. Half the designed amount of the nanopowder was then added, and the mixture was ball-milled (Laboratory Jar Rolling Mill, Paul O. Abbe, USA). Ball

milling parameters have been reported in the authors' previous publication [7]. The remaining nanopowder was evenly separated into five portions, and each portion was added to the bottle once every hour during ball milling. After all nanopowder was added, ball milling continued for 12 h. Then a sieve with an opening size of 250 μm was used to filter the slurry into a beaker, after which the slurry was ready for spray freeze drying. The spray freeze drying consisted of two steps: spray freezing and freeze drying. The procedures have been reported in the authors' previous publication [7]. The parameters for spray freezing and freeze drying are listed in Table 1. After spray freeze drying, the granulated powder was sieved to obtain a granule size range of 53–90 μm by a sieve shaker (AS 200, Retsch GmbH, Germany). A scanning electron microscope (SEM, TESCAN VEGA II LSU, Czech Republic) was used to characterize the granulated powder. Afterward, the granule size distribution was analyzed with ImageJ. The volume-weighted mean granule size was then obtained.

Table 1. Parameters for spray freeze drying

Step	Parameter	Value
Spray freezing	Compressed air pressure (bar)	0.3
Spray freezing	Slurry feed rate (L/h)	0.5
Freeze drying	Vacuum (mbar)	1.5
Freeze drying	Tray temperature (°C)	20
Freeze drying	Ice collector temperature (°C)	-50
Freeze drying	Drying time (h)	24

2.3 Flowability measurement

Seven different flowability metrics, as listed in Table 2, were measured for all three powders. All measurements were repeated three times for each powder.

Table 2. Flowability metrics and acronyms

Flowability metric	Acronym
Apparent density	AD
Tap density	TD
Volumetric flow rate	VFR
Mass flow rate	MFR
Hausner ratio	HR
Carr index	CI
Repose angle	RA

2.3.1 Apparent density and tap density

Apparent density (AD) is the density of freely settled powder. A Hall flowmeter, as illustrated in Figure 1(a) [24], was used to obtain the AD of the micropowder and granulated powder. As the nanopowder could not freely fall through the Hall funnel (with an opening diameter of 2.5 mm), a Carney funnel (with an opening diameter of 5.0 mm) was used to measure its AD with other conditions kept the same [25]. The mass of the empty density cup was recorded firstly. Afterward, the funnel was filled with powder while the funnel opening was blocked. The powder was then let fall, filled the cup beneath the funnel, formed a cone in the cup, and eventually overflowed from the cup. The cone was gently wiped off with a spatula, followed by weighting the cup with the powder inside. The net powder mass inside the cup was divided by the cup volume (25 cm^3, as predefined in the standard [24]) to obtain the AD of each powder.

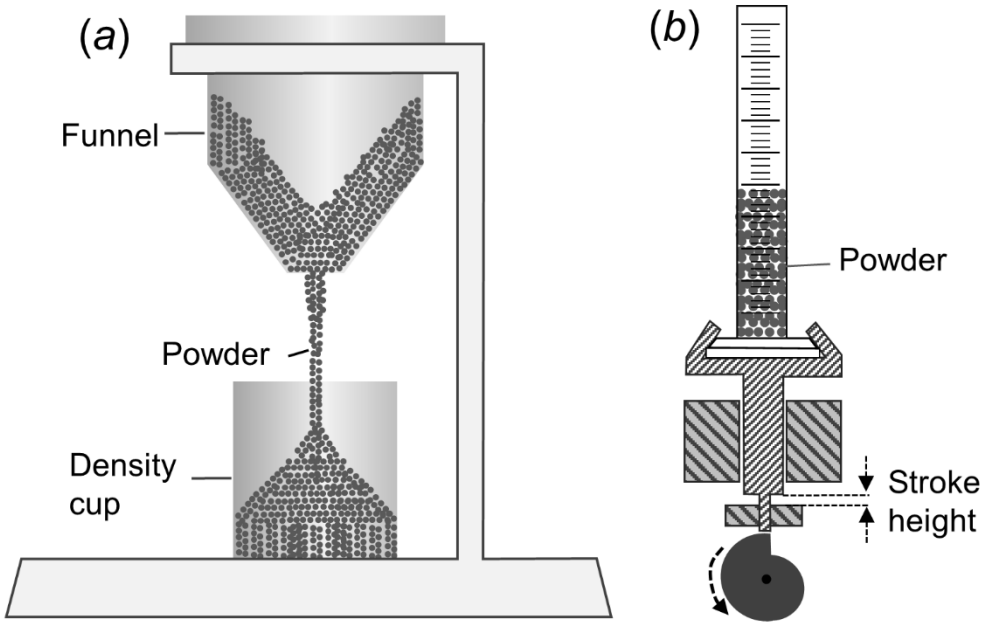

Figure 1. Schematics of (a) Hall flowmeter and (b) tap density meter

Tap density (TD) is the density of a powder that has been tapped, to settle contents, in a container under specified conditions [26]. As the nanopowder and granulated powder have a low density, 50 g of each powder (i.e., the powder mass specified by the standard for TD measurement [26]) had a larger volume than 100 mL (i.e., the volume of the graduated cylinder specified by the same standard [26]). Therefore, each of all three powders was filled into the cylinder to a certain volume. Specifically, TD measurement started by weighting an empty graduated cylinder with a capacity of 100 mL. Afterward, 50 mL of powder was added into the cylinder. The cylinder with powder was then tapped 3000 times with a stroke height of 3 mm by a tap density meter, as shown in Figure 1(b). The tapped volume of each powder was then recorded. The net powder mass inside the cylinder was divided by the tapped volume to obtain the TD of each powder.

2.3.2 Volumetric and mass flow rates

Volumetric and mass flow rates (VFR and MFR, respectively), i.e., the volume and mass of the powder falling through a funnel in unit time, respectively, were measured by the same Hall flowmeter as shown in Figure 1(a). The measurement started with blocking the funnel opening with a piece of tape. Since both the nanopowder and granulated powder have a low density, 50 g of each powder, which is the specified powder mass in the measurement standard [27], has a larger volume than the funnel capacity. Therefore, when all three powders were measured, the funnel was filled to full instead of to a specified mass. To determine the net volume inside the funnel, the funnel was filled with water, followed by measuring the funnel mass with water in it. The net water mass was divided by the water density at the measurement temperature to calculate the net volume, which is the same as the net powder volume. The funnel was then filled with the powder until it overflowed from the periphery of the funnel. Afterward, the powder above the top surface was gently wiped off by a spatula, followed by weighting the funnel and the powder inside. Then the mass of empty funnel was subtracted from the mass of funnel with powder inside to determine the net powder mass. The time that the powder completely passed through the funnel was recorded. The net powder volume and mass inside the funnel were divided by the time to obtain the VFR and MFR, respectively.

2.3.3 Hausner ratio and Carr index

Hausner ratio (HR) and Carr index (CI) are two closely-related empirical metrics to assess the powder flowability. They are defined by the following equations [2]:

$$HR = \frac{\rho_t}{\rho_a} \tag{1}$$

$$CI = 100\left(1 - \frac{\rho_a}{\rho_t}\right) \tag{2}$$

where ρ_t and ρ_a are absolute TD and AD, respectively.

2.3.4 Repose angle

The Hall flowmeter, as illustrated in Figure 1(a), was used to measure the repose angle (RA) of the micropowder and granulated powder [28] while a Carney funnel for the nanopowder because it could not freely fall through the Hall funnel. The funnel opening was blocked first, followed by filling the funnel with powder. Afterward, the powder fell through the funnel, filled the cup beneath the funnel, formed a cone in the cup, and eventually overflowed from the cup. The diameter of the cone base (d) and the height of the cone (H) were measured by imaging the cone and processing the images with ImageJ. The following equation was used to calculate the RA (θ):

$$\theta = \tan^{-1}(2H/d) \tag{3}$$

2.4 Sinterability measurement

Sinterability has different definitions in the literature [29–31]. In this study, it is considered as one of the powder properties. Therefore, the sinterability measurement procedures were purposefully designed to press the powder into a disk to reach a high green density before sintering. In this way, the sintering process started from a favorable initial state, unleashing the full densification potential of the powder.

Three different sinterability metrics, as listed in Table 3, were measured for all three powders. All measurements were repeated three times for each powder.

Table 3. Sinterability metrics and acronyms

Sinterability metric	Acronym
Sintered bulk density	SBD
Volumetric shrinkage	VS
Densification ratio	DR

2.4.1 Sintered bulk density

Green disk samples were firstly prepared. For each sample, 1 g of powder was pressed at 100 MPa into a cylindrical disk of Φ12.7 mm by a hydraulic cold press (Carver Laboratory Press, Model C, Fred S. Carver Inc., USA). The disk sample from the micropowder collapsed after pressing. Therefore, an aqueous solution containing 3 wt. % polyvinyl alcohol (PVA, 363138, Sigma-Aldrich, USA) was added to the micropowder as a binder. The micropowder and the binder solution were mixed at a mass ratio of 99.5:0.5. Since the PVA percentage is low, its effect on sintering of disk samples from the micropowder could be neglected. Then the mixture was put in an oven with a temperature of 60 °C for 0.5 h to evaporate the water, followed by pressing.

Sintering of all green disk samples from all three powders was conducted in a bench-top muffle furnace (KSL-1700X-A1-UL, MTI Corp., USA). The sintering temperature was 1600 °C, ramp rate was 5 °C/min, and sintering time was 2 h. The samples were cooled inside the furnace to room temperature after sintering.

Sintered bulk density (SBD) of the disk samples was measured with the Archimedes method based on an ISO standard [32] using a density measurement kit (Torbal AGCN200, Scientific Industries Inc., USA). A schematic of the measurement process is shown in Figure 2. Specifically, the dry mass of the sintered sample (m_{s1}) was firstly measured. Then the sample was boiled in

deionized water for 2 h and then cooled to room temperature. This step allowed the open pores to be filled with water. The immersed mass of the sintered sample (m_{s2}) was measured. Afterward, the sample was wiped with a wet cloth to remove the water droplets on the surface. The cloth was previously saturated by water completely to avoid drawing out the water from the open pores of the sample. The soaked mass (i.e., the mass of the solid plus the water inside the open pores) of sintered sample (m_{s3}) was lastly measured. The bulk volume (i.e., the volume of the solid, the closed pores, and the open pores) of the sintered sample (V_s) was calculated based on the following equation:

$$V_s = \frac{m_{s3} - m_{s2}}{\rho_{wt}} \tag{4}$$

where ρ_{wt} is the absolute water density at the temperature during the measurement. Finally, the relative sintered bulk density (ρ_s') was calculated with the following equation:

$$\rho_s' = \frac{m_{s1}}{V_s} \cdot \frac{1}{\rho_{th}} \times 100\% \tag{5}$$

where ρ_{th} is the theoretical density of alumina (i.e., 3.97 g/cm^3 [29]).

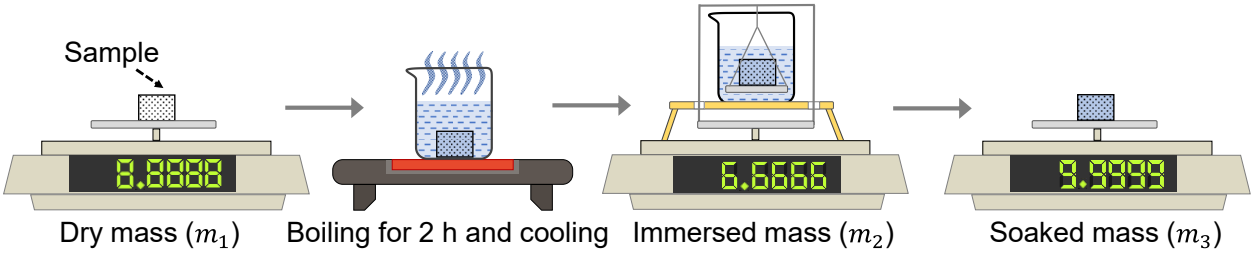

Figure 2. Procedures of the Archimedes method

2.4.2 Volumetric shrinkage and densification ratio

Green bulk volume and density were measured to determine the volumetric shrinkage and

densification ratio. The diameter and thickness of the green disk samples were measured three times at different locations of the sample by a caliper (with an accuracy of 10 μm). Afterward, the green bulk volume (V_g) was calculated.

The volumetric shrinkage (S_V) is the sintering-induced volume reduction divided by the green bulk volume. It was calculated based on the following equation:

$$S_V = \left(\frac{V_g - V_s}{V_g}\right) \times 100\% \tag{6}$$

The mass (m_g) of the green disk samples was measured by a balance. The relative green bulk density (ρ'_g) of the samples was calculated based on the following equation:

$$\rho'_g = \frac{m_g}{V_g} \cdot \frac{1}{\rho_{th}} \times 100\% \tag{7}$$

The densification ratio (R_d) is the ratio of the sintering-induced density increase to the difference between the theoretical density and green bulk density. It was calculated based on the following equation:

$$R_d = \frac{\rho'_s - \rho'_g}{1 - \rho'_g} \times 100\% \tag{8}$$

3 Results and Discussion

3.1 Particle morphology and particle (granule) size of three powders

Figure 3(a) shows the SEM images of some particles from the nanopowder before ball milling. The nanopowder consisted of irregular agglomerates with a wide size range. After ball milling, the large agglomerates were crushed into nanoparticles, as shown in Figure 3(b). The particle size of the nanopowder is about 100 nm.

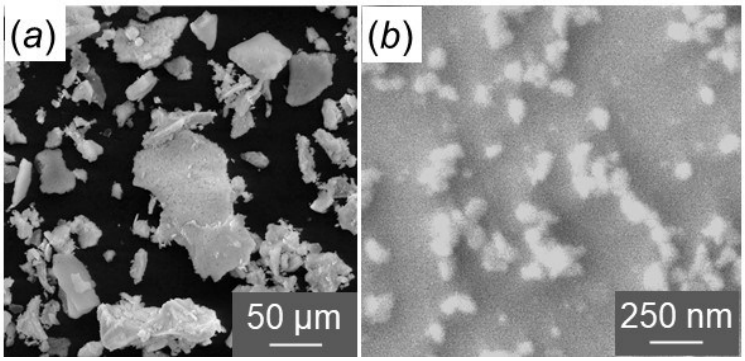

Figure 3. SEM images of nanopowder: (a) before ball milling and (b) after ball milling

Figure 4 shows morphology of the micropowder and granulated powder. Particles in both powders are almost perfectly spherical. Figure 5 shows the particle (granule) size distribution of these two powders. The mean sizes for the micropowder and granulated powder are 77.4 µm and 69.2 µm, respectively.

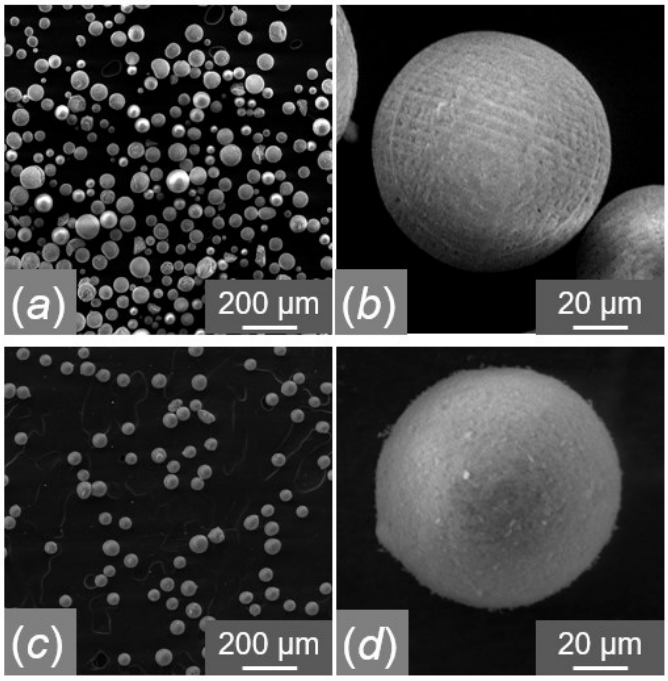

Figure 4. SEM images of some particles from (a) and (b) micropowder, and (c) and (d) granulated powder

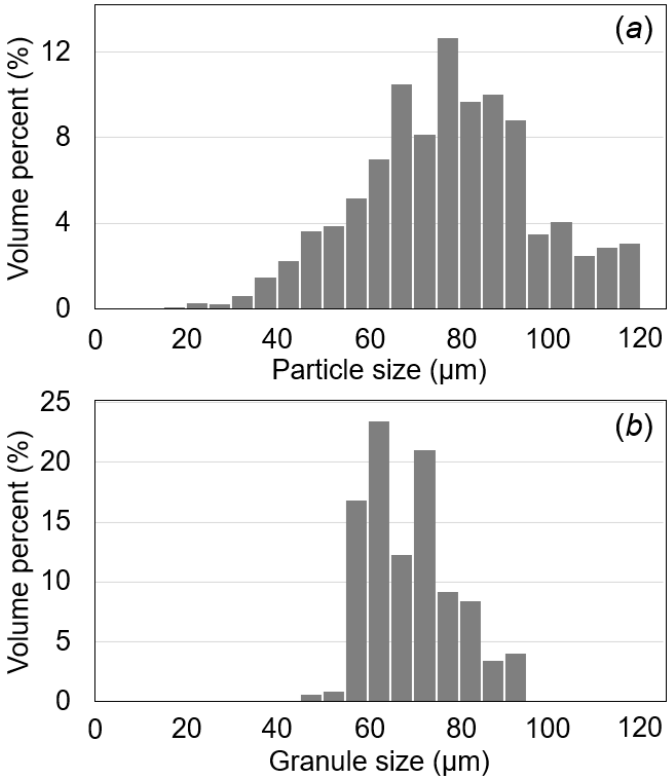

Figure 5. Particle (granule) size distribution of (a) micropowder and (b) granulated powder

3.2 Flowability

3.2.1 Apparent density and tap density

The measured absolute and relative values of apparent density (AD) and tap density (TD) of the three powders are listed in Table 4. The standard deviation was calculated based on three measurements for each powder. Both metrics are basic indexes of bulk density to indicate the powder flowability [33]. A powder with a low flowability has a low bulk density (i.e., low AD and TD). A powder with a high flowability, on the contrary, has a high bulk density (i.e., high AD and TD).

Table 4. Apparent density and tap density of three powders

Powder	Absolute apparent density (g/cm^3)	Relative apparent density (%)	Absolute tap density (g/cm^3)	Relative tap density (%)
Nanopowder	0.29±0.001	7.2±0.03	0.55±0.012	13.8±0.31
Micropowder	2.09±0.004	52.5±0.11	2.38±0.019	59.8±0.47
Granulated powder	0.46±0.006	11.6±0.15	0.56±0.007	14.2±0.17
Granulated powder (monolithic)	/	58.0±3.75	/	71.0±4.25

The comparisons of AD and TD between the nanopowder and granulated powder result in similar findings to the previous study [7]: the nanopowder has a lower AD than the granulated powder while these two powders have a similar TD. However, the hierarchical packing structure of granulated powder was not considered in the previous publication [7]. This consideration is discussed as follows.

The relative AD and TD of the granulated powder (ρ'_{gra}) are governed by the relative packing density of the monolithic granules within the occupied macroscopic space (i.e., intergranular density, ρ'_{interg}) and the relative packing density of nanoparticles within a granule (i.e., intragranular density, ρ'_{intrag}), as schematically illustrated in Figure 6. The relation among these relative packing densities is given by:

$$\rho'_{gra} = \rho'_{interg} \cdot \rho'_{intrag} \tag{9}$$

As granules are the smallest units when a granulated powder flows, relative AD and TD of monolithic granules should be assessed for evaluating its flowability. Therefore, the relative AD and TD of monolithic granules (ρ'_{interg}) [34] were calculated by Equation (9), as listed in Table 4.

The relative packing density of nanoparticles within a granule (ρ'_{intrag}) was assumed to be the solid loading of the slurry for spray freezing (20 vol.%). This assumption is fair because of no significant volume change during the freezing and drying processes of the employed granulation method, as experimentally shown in other work [34,35].

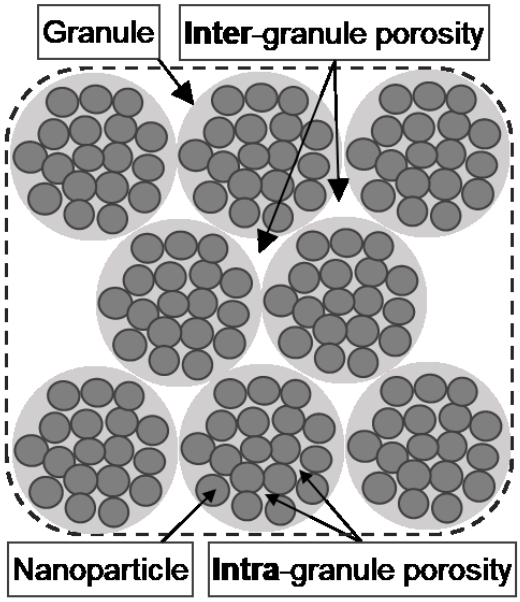

Figure 6. Packing structure of granulated powder

With the hierarchical packing structure of granulated powder considered, the relative AD and TD of the monolithic granules (as shown in Table 4) are much higher than those of the nanopowder. This finding makes sense considering the severe agglomeration and irregular agglomerate shape of the nanopowder.

The relative AD of the monolithic granules, 58.0%, is higher than that of the micropowder, 52.5%. The relative TD of the monolithic granules, 71.1%, is also higher than that of the micropowder, 59.8%. The difference in relative TD (11.3%) between these two powders is larger than that in relative AD (5.5%). It could be attributed to the porous structure and thus low strength of the granules. This can lead to plastic deformation and fracture of the granules [36] during the

tapping, decreasing the intergranular porosity and increasing the packing density of the monolithic granules.

3.2.2 Volumetric and mass flow rates

The volumetric and mass flow rates (VFR and MFR, respectively) of the three powders are listed in Table 5. It should be noted that VFR and MFR cannot be measured for the nanopowder due to the dominant interparticle cohesion and large interagglomerate friction. Therefore, the volumetric and mass flow rates are not suitable metrics to characterize the flowability of the nanopowder.

Table 5. Volumetric and mass flow rates of three powders

Powder	Volumetric flow rate (cm^3/s)	Mass flow rate (g/s)
Nanopowder	/	/
Micropowder	0.70±0.01	1.54±0.01
Granulated powder	0.30±0.01	0.15±0.01

The micropowder has a VFR value that is about twice that of the granulated powder. This could be explained by their different apparent densities. As the powder was freely settled in the funnel before the measurements of flow rates, the absolute powder packing density in the funnel (ρ_f, 2.19 g/cm^3 and 0.48 g/cm^3 for the micropowder and granulated powder, respectively) was close to the absolute AD (ρ_a, 2.09 g/cm^3 and 0.46 g/cm^3 for the micropowder and granulated powder, respectively). The micropowder has a larger AD and thus a larger gravity-induced pressure at the funnel opening. Therefore, the micropowder has a larger VFR.

The difference in MFR between the micropowder and granulated powder is more significant than that in VFR. This could be explained by the relationship among MFR, VFR, and absolute powder packing density in the funnel (approximately, absolute AD) as follows:

$$Q_m = Q_V \cdot \rho_f \approx Q_V \cdot \rho_a \tag{10}$$

where Q_m is the MFR, Q_V is the VFR, ρ_f is the absolute powder packing density in the funnel, and ρ_a is the absolute AD. This equation suggests that the difference in MFR between two powders is actually a product of differences in both VFR and AD. It means that MFR is even more dependent on AD. Since both the VFR and MFR are heavily dependent on the powder packing density itself, they are not suited for comparing the flowability of different powders.

3.2.3 Hausner ratio and Carr index

Both Hausner ratio (HR) and Carr index (CI) represent the difference between AD and TD. When AD is measured, a cohesive powder (i.e., of a low flowability) obtains a loose packing structure after free falling from the funnel while a free-flowing powder (i.e., of a high flowability) obtains a relatively dense packing structure [33]. When TD is measured, the loose packing structure of a cohesive powder (i.e., of a low flowability) changes under tapping and its packing density increases significantly, resulting in a large difference between the AD and TD. On the contrary, a free-flowing powder (i.e., of a high flowability) has little room for further rearrangement due to the already dense packing structure induced by gravity during free falling, and thus its packing density only slightly increases after tapping [33].

Table 6 lists the HR and CI values of the three powders. Based on the definition, the smaller the HR (i.e., closer to one), the better the flowability. Both the micropowder and granulated powder achieved relatively small HR values while the nanopowder had a relatively large HR value. For

CI, the same rule applies: the smaller the CI (i.e., closer to zero), the better the flowability. Similar trends were observed on CI. It should be noted that the HR and CI values of the granulated powder are slightly higher than those of the micropowder. One possible reason is the plastic deformation or fracture of the granules during tapping and thus an unusually high tap density of the monolithic granules (as listed in Table 4).

Table 6. Hausner ratio and Carr index of three powders

Powder	Hausner ratio	Carr index
Nanopowder	1.93±0.04	48.15±0.96
Micropowder	1.14±0.01	12.17±0.58
Granulated powder	1.23±0.02	18.66±1.20

3.2.4 Repose angle

Table 7 and Figure 7 show the repose angle (RA) values of all three powders. The granulated powder achieved an RA close to that of the micropowder. Both the RA values of these two powders are much smaller than that of the nanopowder. This is probably due to the much less interparticle (or intergranular) cohesion.

Table 7. Repose angle of three powders

Powder	Repose angle (°)
Nanopowder	67.80±5.80
Micropowder	25.22±0.59
Granulated powder	29.88±0.49

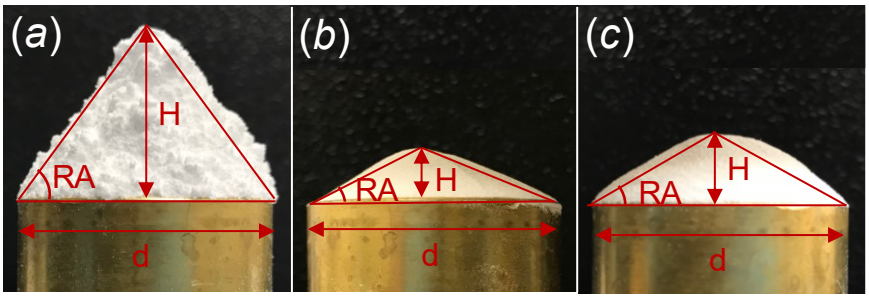

Figure 7. Measurements of repose angle for (a) nanopowder, (b) micropowder, and (c) granulated powder

3.2.5 Summary of flowability

Normalized values for five flowability metrics are summarized in Figure 8. Flowability values of the micropowder were set as the baseline to obtain the normalized values of each flowability metric for clear comparisons among different powders. High flowability is associated with large AD and TD and small HR, CI, and RA. The VFR and MFR are not summarized because they are not suitable for comparing the flowability of different powders as discussed in Section 3.2.2.

All flowability metrics show a large difference between the nanopowder and micropowder while a small difference between the micropowder and granulated powder. Specifically, AD and TD suggest the flowability of the granulated powder is slightly higher than that of the micropowder while HR, CI, and RA suggest the opposite. These results indicate the flowability of the granulated powder is comparable to that of the micropowder.

Moreover, the consideration of the hierarchical packing structure of granulated powder makes AD and TD more appropriate for comparing its flowability with other powders. With this consideration, AD and TD of granulated powder are significantly larger than those of the nanopowder, which agrees with the results of other flowability metrics.

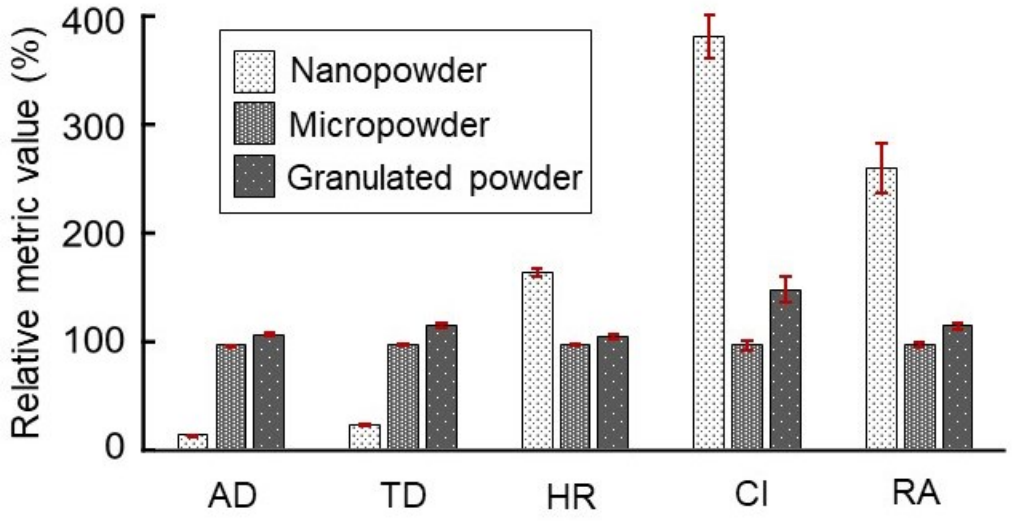

Figure 8. Normalized values for different flowability metrics, including apparent density (AD), tap density (TD), Hausner ratio (HR), Carr index (CI), and repose angle (RA)

3.3 Sinterability

3.3.1 Sintered bulk density

Results for relative sintered bulk density (SBD) are listed in Table 8. As a smaller particle size corresponds to a higher sintering driving force, more significant densification occurred for the nanopowder and granulated powder than the micropowder, leading to higher SBD values. The relative SBD values of the granulated powder and the nanopowder are close since the granulated powder has the same primary particle size (i.e., ~100 nm) as the nanopowder.

Table 8. Relative sintered bulk density of three powders

Powder	Relative sintered bulk density (%)
Nanopowder	89.7±0.8
Micropowder	62.4±2.7
Granulated powder	96.9±1.3

3.3.2 Volumetric shrinkage and densification ratio

Results for volumetric shrinkage (VS) and densification ratio (DR) are listed in Table 9. The nanopowder and granulated powder have comparably large values of VS, indicating the high sinterability of these two powders. The micropowder has only a limited VS value, suggesting the low sinterability of the micropowder. Similarly, the nanopowder and granulated powder have much higher DR values than the micropowder. Both VS and DR values of the granulated powder are close to those of the nanopowder as the granulated powder has the same primary particle size (i.e., ~100 nm) as the nanopowder.

Table 9. Volumetric shrinkage and densification ratio of three powders

Powder	Volumetric shrinkage (%)	Densification ratio (%)
Nanopowder	61.2±1.6	83.9±2.3
Micropowder	5.2±3.7	7.1±1.0
Granulated powder	57.2±1.4	94.5±1.9

3.3.3 Summary of sinterability

All sinterability metrics, as summarized in Figure 9, show a large difference between the nanopowder and micropowder while a small difference between the nanopowder and granulated powder. Specifically, SBD and DR suggest the sinterability of the granulated powder is slightly higher than that of the nanopowder while VS suggests the opposite. This indicates that the sinterability of the granulated powder is comparable to that of the nanopowder.

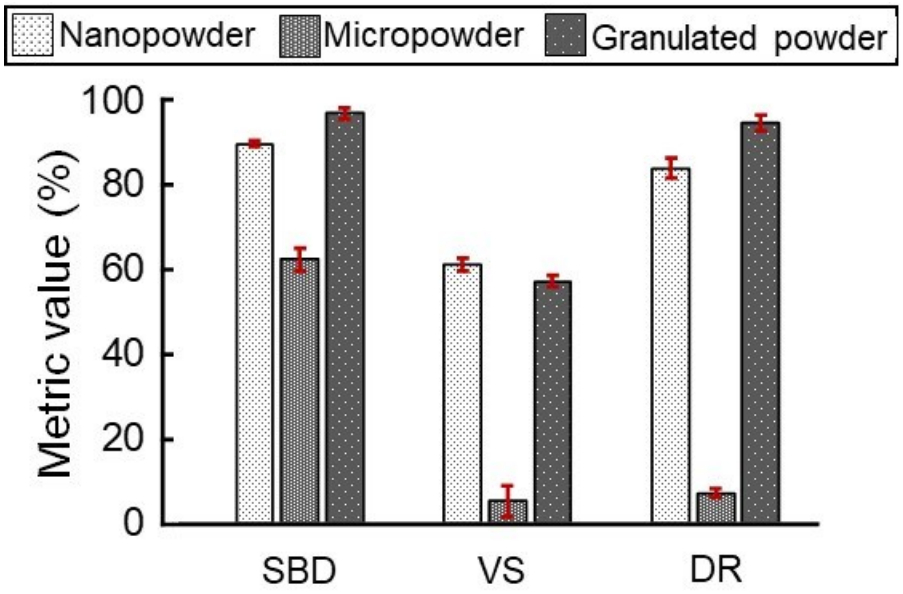

Figure 9. Sinterability results of three powders, including relative sintered bulk density (SBD), volumetric shrinkage (VS), and densification ratio (DR)

4 Conclusions

This study compares the flowability and sinterability of three types of feedstock powders for binder jetting additive manufacturing, i.e., nanopowder, micropowder, and granulated powder. Various flowability metrics employed include apparent density, tap density, volumetric flow rate, mass flow rate, Hausner ratio, Carr index, and repose angle. Various sinterability metrics employed include sintered bulk density, volumetric shrinkage, and densification ratio.

Experimental data on all metrics indicate that the nanopowder has a significantly lower flowability than the micropowder and granulated powder (with the hierarchical packing structure considered). The flowability comparison between the granulated powder and micropowder using different metrics has slightly different results. Results on apparent density and tap density indicate that the flowability of the granulated powder is slightly higher while results on Hausner ratio, Carr index, and repose angle indicate that the flowability of the micropowder is slightly higher.

Therefore, it is concluded that these two powders have a comparable flowability. Moreover, the consideration of the hierarchical packing structure of the granulated powder makes apparent density and tap density more appropriate for comparing its flowability with other powders.

Experimental data on all metrics indicate that the micropowder has a significantly lower sinterability than the granulated powder and nanopowder. The sinterability comparison between the granulated powder and nanopowder using different metrics has slightly different results. Experimental data on sintered bulk density and densification ratio indicate that the sinterability of the granulated powder is slightly higher while experimental data on volumetric shrinkage indicate that the sinterability of the nanopowder is slightly higher. Therefore, it is concluded that these two powders have a comparable sinterability.

In a nutshell, the micropowder has a high flowability but a low sinterability, the nanopowder has a low flowability but a high sinterability, and the granulated powder has both a high flowability and a high sinterability.

This comparison study of flowability and sinterability among nonopowder, micropower, and gtranulate powder has follwing impacts on binder jetting: (1) it can guide the selection of a proper feedstock powder to avoid spreading-induced defects and achieve a desired printed and sintered density; (2) it confirms that granulated powder has relatively high flowability and high sinterability, and is a promising binder jetting feedstock powder.

Acknowledgements

This material is based upon work supported by the National Science Foundation under Grant No. 1762341. The authors acknowledge Mr. Martin Sjöstedt from PowderPro AB for his helpful advice about the slurry preparation.

References

[1] ASTM International/International Standard, 2015, "ISO/ASTM 52900:2015 - Additive Manufacturing — General Principles — Terminology."

[2] Du, W., Ren, X., Pei, Z., and Ma, C., 2020, "Ceramic Binder Jetting Additive Manufacturing: A Literature Review on Density," Journal of Manufacturing Science and Engineering, **142**(4), pp. 1–66.

[3] Li, M., Du, W., Elwany, A., Pei, Z., and Ma, C., 2020, "Metal Binder Jetting Additive Manufacturing: A Literature Review," Journal of Manufacturing Science and Engineering, **142**(9), pp. 1–45.

[4] Qian, C., and Sun, J., 2013, "Fabrication of the Porous Hydroxyapatite Implant by 3D Printing," Journal of Ceramic Processing Research, **14**(4), pp. 513–516.

[5] Tarafder, S., Davies, N. M., Bandyopadhyay, A., and Bose, S., 2013, "3D Printed Tricalcium Phosphate Bone Tissue Engineering Scaffolds: Effect of SrO and MgO Doping on in Vivo Osteogenesis in a Rat Distal Femoral Defect Model," Biomaterials Science, **1**(12), pp. 1250–1259.

[6] Tarafder, S., Dernell, W. S., Bandyopadhyay, A., and Bose, S., 2015, "SrO- and MgO-Doped Microwave Sintered 3D Printed Tricalcium Phosphate Scaffolds: Mechanical Properties and in Vivo Osteogenesis in a Rabbit Model," Journal of Biomedical Materials Research - Part B Applied Biomaterials, **103**(3), pp. 679–690.

[7] Miao, G., Du, W., Moghadasi, M., Pei, Z., and Ma, C., 2020, "Ceramic Binder Jetting Additive Manufacturing: Effects of Granulation on Properties of Feedstock Powder and Printed and Sintered Parts," Additive Manufacturing, **36**, p. 101542.

[8] Bai, Y., Wagner, G., and Williams, C. B., 2015, "Effect of Bimodal Powder Mixture on Powder Packing Density and Sintered Density in Binder Jetting of Metals," *International Solid Freeform Fabrication Symposium*, Austin, TX, pp. 758–771.

[9] Butscher, A., Bohner, M., Roth, C., Ernstberger, A., Heuberger, R., Doebelin, N., Rudolf Von Rohr, P., and Müller, R., 2012, "Printability of Calcium Phosphate Powders for Three-Dimensional Printing of Tissue Engineering Scaffolds," Acta Biomaterialia, **8**(1), pp. 373–385.

[10] Zocca, A., Gomes, C. M., Bernardo, E., Muller, R., Gunster, J., and Colombo, P., 2013, "LAS Glass-Ceramic Scaffolds by Three-Dimensional Printing," Journal of the European Ceramic Society, **33**(9), pp. 1525–1533.

[11] Lanzetta, M., and Sachs, E., 2001, "The Line Formation with Alumina Powders in Drop on Demand Three Dimensional Printing," *The First International Seminar on Progress in Inovative Manufacturing Engineering*, Sestri Levante, pp. 197–204.

[12] Sun, C., Tian, X., Wang, L., Liu, Y., Wirth, C. M., Günster, J., Li, D., and Jin, Z., 2017, "Effect of Particle Size Gradation on the Performance of Glass-Ceramic 3D Printing Process," Ceramics International, **43**(1), pp. 578–584.

[13] Du, W., Ren, X., Chen, Y., Ma, C., Radovic, M., and Pei, Z., 2018, "Model Guided Mixing of Ceramic Powders with Graded Particle Sizes in Binder Jetting Additive Manufacturing," *ASME 2018 13th International Manufacturing Science and Engineering Conference*, College Station, TX, pp. 1–9.

[14] Du, W., Roa, J., Hong, J., Liu, Y., Pei, Z., and Ma, C., 2021, "Binder Jetting Additive Manufacturing: Effect of Particle Size Distribution on Density," Journal of Manufacturing Science and Engineering, **143**(9), pp. 091002_1–091002_26.

[15] Suwanprateeb, J., Sanngam, R., and Panyathanmaporn, T., 2010, "Influence of Raw Powder Preparation Routes on Properties of Hydroxyapatite Fabricated by 3D Printing Technique," Materials Science and Engineering C, **30**(4), pp. 610–617.

[16] Irsen, S. H., Leukers, B., Höckling, C., Tille, C., and Seitz, H., 2006, "Bioceramic Granulates for Use in 3D Printing: Process Engineering Aspects," Materialwissenschaft und Werkstofftechnik, **37**(6), pp. 533–537.

[17] Gildenhaar, R., Knabe, C., Gomes, C., Linow, U., Houshmand, A., and Berger, G., 2011, "Calcium Alkaline Phosphate Scaffolds for Bone Regeneration 3D-Fabricated by Additive Manufacturing," Key Engineering Materials, **493**, pp. 849–854.

[18] Ben, Y., Zhang, L., Wei, S., Zhou, T., Li, Z., Yang, H., Wang, Y., Selim, F. A., Wong, C., and Chen, H., 2017, "PVB Modified Spherical Granules of β-TCP by Spray Drying for 3D Ceramic Printing," Journal of Alloys and Compounds, **721**, pp. 312–319.

[19] Seitz, H., Deisinger, U., Leukers, B., Detsch, R., and Ziegler, G., 2009, "Different Calcium Phosphate Granules for 3-D Printing of Bone Tissue Engineering Scaffolds," Advanced Engineering Materials, **11**(5), pp. 41–46.

[20] Cox, S. C., Thornby, J. A., Gibbons, G. J., Williams, M. A., and Mallick, K. K., 2015, "3D Printing of Porous Hydroxyapatite Scaffolds Intended for Use in Bone Tissue Engineering Applications," Materials Science and Engineering C, **47**, pp. 237–247.

[21] Chumnanklang, R., Panyathanmaporn, T., Sitthiseripratip, K., and Suwanprateeb, J., 2007, "3D Printing of Hydroxyapatite: Effect of Binder Concentration in Pre-Coated Particle on Part Strength," Materials Science and Engineering C, **27**(4), pp. 914–921.

[22] Du, W., Miao, G., Liu, L., Pei, Z., and Ma, C., 2019, "Binder Jetting Additive Manufacturing of Ceramics: Feedstock Powder Preparation by Spray Freeze Granulation," *ASME 2019 14th International Manufacturing Science and Engineering Conference*, Errie, PA, pp. 1–6.

[23] Du, W., Miao, G., Liu, L., Pei, Z., and Ma, C., 2019, "Binder Jetting Additive Manufacturing of Ceramics: Comparison of Flowability and Sinterability between Raw and Granulated Powders," *ASME 2019 14th International Manufacturing Science and Engineering Conference*, Errie, PA, pp. 1–8.

[24] ASTM International, 2017, "B212-17: Standard Test Method for Apparent Density of Free-Flowing Metal Powders Using the Hall Flowmeter Funnel."

[25] ASTM International, 2013, "B417 2013: Standard Test Method for Apparent Density of Non-Free-Flowing Metal Powders Using the Carney Funnel."

[26] ASTM International, 2015, "B527-15: Standard Test Method for Tap Density of Metal Powders and Compounds."

[27] ASTM International, 2017, "B213-17: Standard Test Methods for Flow Rate of Metal Powders Using the Hall Flowmeter."

[28] ASTM International, 2000, "C 1444-00: Standard Test Method for Measuring the Angle of Repose of Free-Flowing Mold Powders."

[29] Kang, S.-J. L., 2005, *Sintering : Densification, Grain Growth, and Microstructure*, Elsevier Butterworth-Heinemann, Burlington.

[30] Hwang, H. J., Yasuoka, M., Sando, M., Toriyama, M., and Niihara, K., 1999, "Fabrication, Sinterability, and Mechanical Properties of Lead Zirconate Titanate/Silver Composites," Journal of the American Ceramic Society, **82**(9), pp. 2417–2422.

[31] Lara, C., Pascual, M. J., and Durán, A., 2004, "Glass-Forming Ability, Sinterability and Thermal Properties in the Systems RO-BaO-SiO2 (R = Mg, Zn)," Journal of Non-Crystalline Solids, **348**(15), pp. 149–155.

[32] ISO, 2013, "ISO 18754:2013 Fine Ceramics (Advanced Ceramics, Advanced Technical Ceramics) – Determination of Density and Apparent Porosity."

[33] Abdullah, E. C., and Geldart, D., 1999, "The Use of Bulk Density Measurements as Flowability Indicators," Powder Technology, **102**(2), pp. 151–165.

[34] Oberacker, R., 2011, “Powder Compaction by Dry Pressing,” *Ceramic Science and Technology, Volume 3: Synthesis and Processing*, R. Riedel, and I.-W. Chen, eds., John Wiley & Sons, pp. 10–14.

[35] Adolfsson, E., and Shen, Z., 2012, “Effects of Granule Density on Strength and Granule Related Defects in Zirconia,” Journal of the European Ceramic Society, **32**(11), pp. 2653–2659.

[36] Cheong, Y. S., Mangwandi, C., Fu, J., Adams, M. J., Hounslow, M. J., and Salman, A. D., 2007, “A Mechanistic Description of Granule Deformation and Breakage,” Handbook of Powder Technology, **12**, pp. 1055–1120.